Ultra-high resolution microwave photonic radar with post-bandwidth synthesis

Cong Ma (马 丛), Hao Chen (陈 浩), Xingwei Ye (叶星炜), Xiangchuan Wang (王祥传), and Shilong Pan (潘时龙)*

Key Laboratory of Radar Imaging and Microwave Photonics, Ministry of Education, Nanjing University of Aeronautics and Astronautics, Nanjing 210016, China

**Corresponding author: pans@nuaa.edu.cn*

Received December 16, 2019; accepted March 25, 2020; posted online May 22, 2020

We demonstrate microwave photonic radar with post-bandwidth synthesis, which can realize target detection with ultra-high range resolution using relatively small-bandwidth radio frequency (RF) frontends. In the proposed radar, two temporal-overlapped linear frequency-modulated (LFM) signals with the same chirp rate and different center frequencies are transmitted. By post-processing the de-chirped echoes in the receiver, a signal equivalent to that de-chirped from an LFM signal with the combined bandwidth is achieved. In a proof-of-concept experiment, two LFM signals with bandwidths of 8.4 GHz are exploited to achieve radar detection with an equivalent bandwidth of 16 GHz, and a range resolution of 1 cm is obtained.

Keywords: microwave photonics; ultra-high resolution; synthetic bandwidth.
doi: 10.3788/COL202018.072501.

High-resolution radars are highly desirable in military and civil applications[1]. To realize the high resolution, linear frequency-modulated (LFM) signals with large bandwidth are used[2,3]. However, the generation and processing of the large-bandwidth LFM signals create great challenges for the state-of-the-art electronic technologies[4,5]. Due to the distinct features of photonic devices, such as wide bandwidth, low transmission loss, and electromagnetic interference immunity, microwave photonic technologies were proposed to enhance radar systems[6–21]. Spectral shaping and frequency to time mapping (FTTM)[14–16] were used to generate broadband LFM signals. However, the time-bandwidth product (TBWP) of the LFM signal is usually small, which is not suitable for radar applications in long distance detection. To improve the TBWP, a variety of microwave photonic signal generation architectures were proposed. For example, a logic-operation-based photonic digital-to-analog converter can be used to generate a wideband LFM signal with small timing jitter[17], and photonic frequency multiplication can also be applied to obtain large carrier frequency and bandwidth[18–21]. However, despite how broad bands the photonic approaches are with, the limited bandwidth of the radio frequency (RF) frontends and antennas would hinder further increase of the resolution.

A possible solution is to apply sparse multi-band signals[22,23]. Unfortunately, the continuous spectral profile of a target cannot be obtained directly, and complex algorithms should be used to fill the spectral gaps[24,25]. Even so, fake peaks in the range profile of the target may be caused, and the huge amount of calculation is difficult to meet the demands of fast or real-time detection. Another method is bandwidth synthesis, in which two or more narrowband LFM signals with different center frequencies but no spectral gap can be combined as if only one broadband LFM signal is transmitted[26–29]. Until now, lots of efforts devoted by researchers in the electrical area have verified the feasibility of bandwidth synthesis. Nevertheless, the achieved resolution is in the order of decimeters[28].

In this Letter, we demonstrate microwave photonic radar with post-bandwidth synthesis, in which polarization multiplexing and post-bandwidth synthesis are adopted to achieve a large operational bandwidth with relatively small-bandwidth RF frontends, so an ultra-high range resolution can be obtained. In the transmitter, photonic frequency doubling of two intermediate frequency (IF)-LFM signals with different center frequencies is implemented to generate two temporal-overlapped broadband transmitted signals, and, in the receiver, the separation and de-chirping of the temporal-overlapped radar echoes are implemented by photonic frequency mixing. The low-frequency de-chirped signals can be sampled by low-speed analog-to-digital converters (ADCs) and combined into a signal equivalent to the result de-chirped from a synthesized LFM signal with a large bandwidth by a bandwidth synthesis algorithm. Therefore, ultra-high range resolution detection can be achieved.

Figure 1 shows the schematic diagram of the microwave photonic radar. A light from a laser diode (LD) with a frequency of f_0 is sent to a dual-polarization Mach–Zehnder modulator (DPol-MZM), which is an integrated device consisting of two sub-Mach–Zehnder modulators (MZMs), a polarization rotator (PR), and a polarization beam combiner (PBC). Two electrical IF-LFM signals with different frequencies are separately fed into the RF ports of the two sub-MZMs to modulate the LD output. The IF-LFM signals can be expressed as

$$s_i(t) = V_s \cos[2\pi(f_{ci}t + kt^2/2)], \tag{1}$$

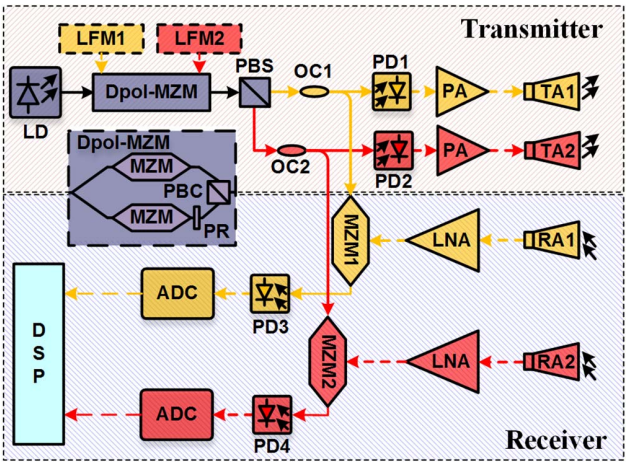

Fig. 1. Schematic diagram of the proposed microwave photonic radar. LD, laser diode; DPol-MZM, dual-polarization Mach–Zehnder modulator; MZM, Mach–Zehnder modulator; PR, polarization rotator; PBC, polarization beam combiner; PBS, polarization beam splitter; OC, optical coupler; PD, photodetector; PA, power amplifier; TA, transmitting antenna; RA, receiving antenna; LNA, low-noise amplifier. Solid line, optical fiber; dashed line, electrical cable. Yellow, channel X; red, channel Y.

where $i = 1$ or 2, and V_s, f_{ci}, and k are the amplitude, the center frequency, and the chirp rate, respectively. The center frequency difference between the two IF-LFM signals is $\Delta f = f_{c2} - f_{c1}$, and the bandwidth is $B = kT$, where T is the pulse width of the LFM signal. The two sub-MZMs are both biased at the minimum transmission point to suppress the optical carrier, so only $\pm 1^{\text{st}}$-order sidebands are obtained. The polarization direction of the signal in the lower branch rotates 90° through the PR. After passing through the PBC, a pair of orthogonally polarized optical signals are obtained at the output of the DPol-MZM. Then, the orthogonally polarized optical signals are sent to a polarization beam splitter (PBS) through an optical fiber and are separated into two polarization channels (X and Y) by the PBS. Each channel is further divided into two by an optical coupler (OC). One branch of each channel is sent to a photodetector (PD). In the PD, the $\pm 1^{\text{st}}$-order sidebands of the optical signal are beaten to generate a frequency-doubled LFM signal, which can be expressed as

$$I_i(t) \propto \cos[2\pi(2f_{ci}t + kt^2)]. \tag{2}$$

The frequency-doubled LFM signals are sent to the transmitting antennas (TAs) for radiation after being amplified by power amplifiers (PAs). The other branch of each channel is sent to an MZM as a reference signal for the receiver.

In the receiver, the echo signals received by the receiving antennas (RAs) are amplified by low-noise amplifiers (LNAs), and then used to drive the MZMs. Here, the MZMs are biased at the quadrature transmission point, and only the optical carrier and $\pm 1^{\text{st}}$-order sidebands are considered. After the MZMs, a frequency pair at $f_0 + (f_{ci} + kt)$ and $f_0 + (f_{ci} + kt) - 2k\tau$ and another frequency pair at $f_0 - (f_{ci} + kt)$ and $f_0 - (f_{ci} + kt) + 2k\tau$ are generated, where τ is the time delay between the radar echo and the transmitted signal. The output of each MZM is sent to a PD. After the PD, the desired de-chirped signal is obtained. It should be noted that the LFM signal transmitted by TA1 (TA2) can also be received by RA2 (RA1), and an undesired signal will be generated. Because the frequency of the signal is much higher than that of the de-chirped signal, a low-frequency PD or an electrical filter can remove it. The two low-frequency de-chirped signals are then sampled by low-speed ADCs to perform signal processing for synthesis in the digital signal processing (DSP) unit. The de-chirped signals can be expressed as

$$r_1(t) \propto \cos[2\pi(2f_{c1}\tau - k\tau^2 + 2k\tau t)], \tag{3}$$

$$\begin{aligned} r_2(t) &\propto \cos[2\pi(2f_{c2}\tau - k\tau^2 + 2k\tau t)] \\ &\propto \cos[2\pi(2f_{c1}\tau - k\tau^2 + 2k\tau t + 2\Delta f\tau)]. \end{aligned} \tag{4}$$

Delaying the signal $r_2(t)$ by a time $T_d = \Delta f/k$, we have

$$r_2(t - T_d) \propto \cos[2\pi(2f_{c1}\tau - k\tau^2 + 2k\tau t)]. \tag{5}$$

Comparing Eq. (3) with Eq. (5), we can see that the two equations are exactly the same, which means that the two de-chirped signals can be combined together to one signal in the time domain. The combined signal is similar to a signal de-chirped from an LFM signal with a bandwidth of $f_T - f_I$, where f_T and f_I are the initial frequency and the terminal frequency of the LFM signals, respectively.

The principle of the post-bandwidth synthesis method is shown in Fig. 2. First, two low-frequency de-chirped signals are obtained. Then, the two low-frequency signals are combined together to obtain a signal equivalent to that de-chirped from an LFM signal with a large bandwidth. It should be noted that the case of $\Delta f < B$ should be satisfied. If $\Delta f \geq B$, it would generate discontinuous phases at the joint points of the synthetic signal because the signal duration after de-chirping is less than T. The phase error at the combination point can be reduced by ensuring the consistency of the device in the two polarization channels. Besides, the different distances between the target and the antennas of the two channels may cause

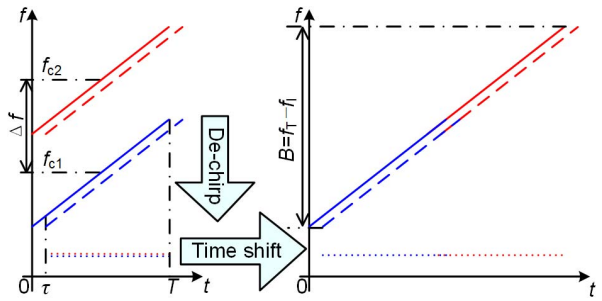

Fig. 2. The principle of the post-bandwidth synthesis. Solid line, the transmitted LFM signals; dashed line, the received LFM signals; dotted line, the de-chirped signals.

additional phase errors, which might be reduced by using an integrated antenna array or compensated by an algorithm[30].

It is well known that the range resolution R of radar is determined by the LFM bandwidth B_L: $R = c/2B_L$, where c is the wave propagation velocity[2]. Therefore, the proposed microwave photonic radar system can achieve an ultra-high range resolution because the equivalent large bandwidth can be obtained by combining the signals de-chirped from the two LFM signals.

To investigate the performance of the proposed system, an experiment is carried out based on the setup in Fig. 1. A light wave at 1550.5 nm with a power of 16 dBm from an LD is sent to a DPol-MZM (Fujitsu FTM7980) via a polarization controller (PC). Two electrical IF-LFM signals generated by an arbitrary waveform generator (AWG) are applied to drive the DPol-MZM in a time-division mode since the AWG only has one channel. The two sub-MZMs of the DPol-MZM are biased at the minimum transmission point. An erbium-doped fiber amplifier (EDFA) is used to amplify the output signal of the DPol-MZM. To reduce the out-of-band spontaneous emission noise of the EDFA, an optical filter is used. The output signal of the optical filter is sent to a PBS via a PC. By adjusting the PC, the polarization directions of the two orthogonally polarized optical signals are aligned with that of the PBS, so that the two optical signals in the orthogonal polarizations are separated. Each optical signal is divided into two branches through a 20:80 OC. One branch of each channel is sent to a 40 GHz PD (u2t XPDV2120RA) to generate the frequency-doubled LFM signal. The LFM signal is amplified by an electrical PA before being sent to a horn antenna for radiation. The optical signal in the other branch is sent to an MZM (Fujitsu FTM7938) as a reference signal. The echo signal collected by the RA is amplified by an LNA and then fed to the MZM. The output signal from the MZM is sent to a 20 GHz PD (Cetc44 GD45216S) followed by a band-pass filter (18–25 MHz) to generate de-chirped signals. To ensure the consistency of the phase in the two polarization channels, the two channels share the same devices in the time-division mode except for the antennas. In the experiment, the waveform of the electrical signal is sampled by a real-time oscilloscope (Keysight DSO-X92504A) and then processed by a computer.

Due to the hardware constraints, the experiment is implemented in a time-division mode, i.e., two LFM signals are transmitted and received at different times. There are two problems that need to be considered for system verification in this way. One problem is that, as discussed in the principle section, when the two LFM signals are used at the same time, the receiver can generate high-frequency signals, which can be removed by using a low-frequency PD or an electrical filter. The other problem is the crosstalk between the orthogonal polarizations. To investigate the crosstalk between the orthogonal polarizations, the signal input to one of the sub-MZMs is disconnected, and the output optical spectrum of the PBS is detected, so we can know the power leakage between the orthogonally polarized optical signals. The results are shown in Fig. 3. As can be seen, the crosstalk between the two polarizations is very weak and can be ignored in the experiment.

First, two IF-LFM signals with center frequencies of 10.525 GHz and 11.475 GHz are generated by the AWG. Both of these signals have a bandwidth of 1.05 GHz and a pulse width of 52.5 μs. After the PD, two LFM signals with center frequencies of 21.05 GHz and 22.95 GHz are obtained at the transmitter, each of which has a bandwidth of 2.1 GHz and a pulse width of 52.5 μs. The instantaneous frequency-time diagrams are shown in Fig. 4. To investigate the performance of the system, a distance measurement experiment is implemented. Two metallic plane targets (6.8 cm × 6.1 cm) spaced 5 cm apart are placed on the perpendicular bisector of the antenna array to minimize the phase error caused by different distances between the antenna and the targets, as shown in Fig. 5. The generated de-chirped signals are sampled by the real-time oscilloscope with a sampling rate of 100 MSa/s.

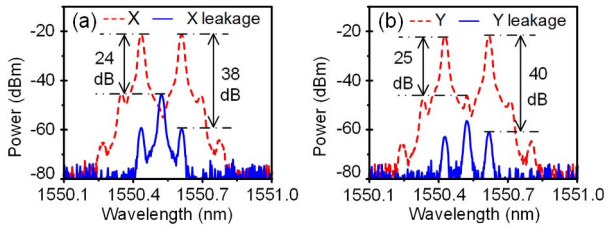

Fig. 3. Optical spectra of the polarized optical signals at (a) channel X and (b) channel Y.

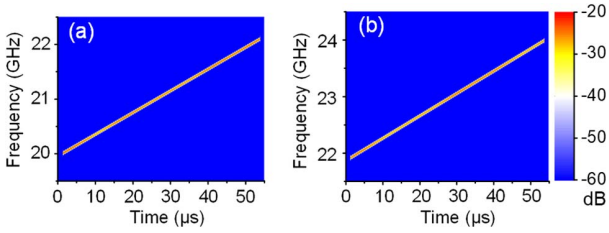

Fig. 4. The frequency-time diagrams of the LFM signals generated in (a) channel X and (b) channel Y.

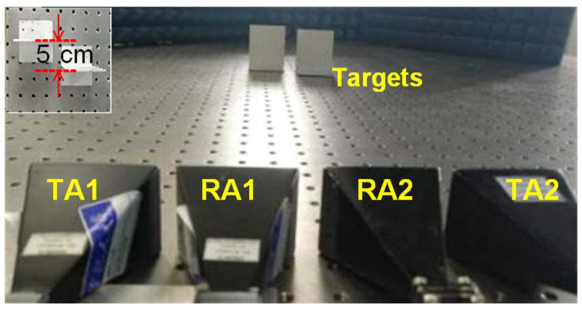

Fig. 5. Picture of the antennas and targets in the experiment. Inset, top-view of the targets.

By applying the fast Fourier transform (FFT), the electrical spectra are obtained, as shown in Figs. 6(a) and 6(b). By combining the two de-chirped signals, the synthetic signal is obtained, and the corresponding spectrum is shown by the red curve in Fig. 6(c). As can be seen, two peaks are located at 22.9474 MHz and 22.9611 MHz, while only one peak can be observed in Figs. 6(a) and 6(b). The frequency difference between the two peaks is 13.7 kHz, and the calculated distance between the two targets is 5.14 cm, which shows that the two targets can be distinguished with an error of 0.14 cm, very close to the real value.

Then, a real LFM signal with a center frequency of 22 GHz, a bandwidth of 4 GHz, and a pulse width of 100 μs is transmitted using one channel of the system. Comparing the obtained waveform of the de-chirped signal with the synthetic waveform, we can see that the real envelope is approximately the same as the synthetic envelope, as shown in Fig. 7. Figs. 7(b), 7(c), and 7(d) are zoom-in views of regions A (9.5–10.5 μs), B (49.5–50.5 μs), and C (89.5–90.5 μs) in Fig. 7(a), respectively. By performing the FFT, the spectrum of the real de-chirped signal is obtained and shown as the blue curve in Fig. 6(c). Again, two peaks at 22.9483 MHz and 22.9621 MHz are observed. The frequency difference between the two peaks is 13.8 kHz, and the calculated distance between the two targets is 5.18 cm. The results further prove that the post-synthesis method is effective.

Finally, we change the two output IF-LFM signals of the AWG to signals with bandwidths of 4.2 GHz and pulse widths of 210 μs at center frequencies of 11.35 GHz and 15.15 GHz. The transmitter can obtain two LFM signals with bandwidths of 8.4 GHz and pulse widths of 210 μs at

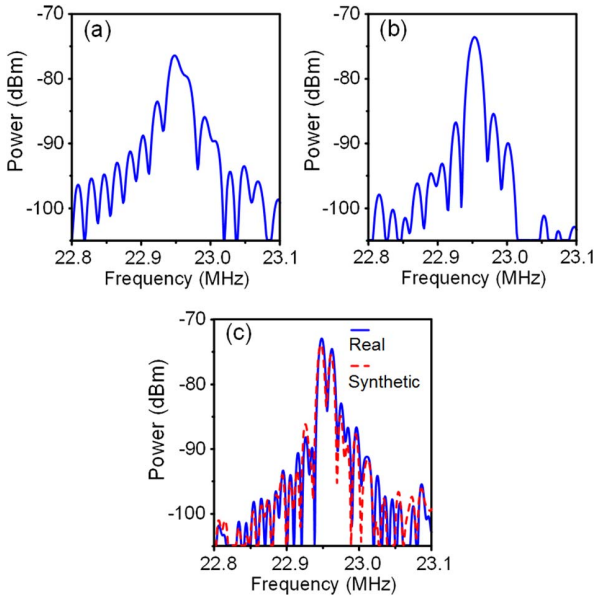

Fig. 6. Spectra of the de-chirped signals generated in (a) channel X and (b) channel Y when two LFM signals with bandwidths of 2.1 GHz are transmitted. (c) Comparison between the spectra obtained by a real 4 GHz signal and the synthetic signal.

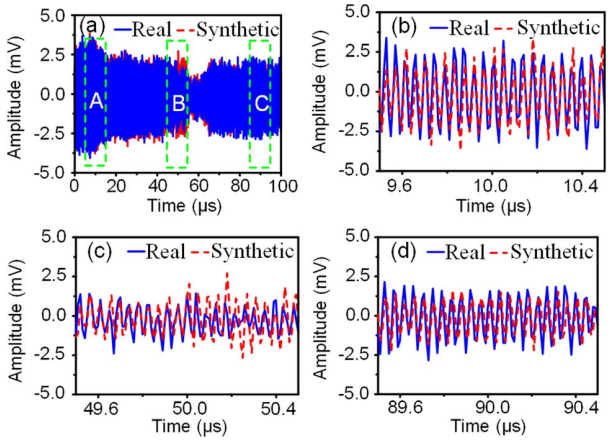

Fig. 7. (a) Comparison between the waveforms of the real and synthetic de-chirped signals. (b), (c), (d) Zoom-in views of the regions A, B, and C in (a).

center frequencies of 22.7 GHz and 30.3 GHz. In order to verify the high-resolution performance of the system, two metallic planes with a spacing of 1 cm are used as the target. Two signals de-chirped from the two LFM signals are

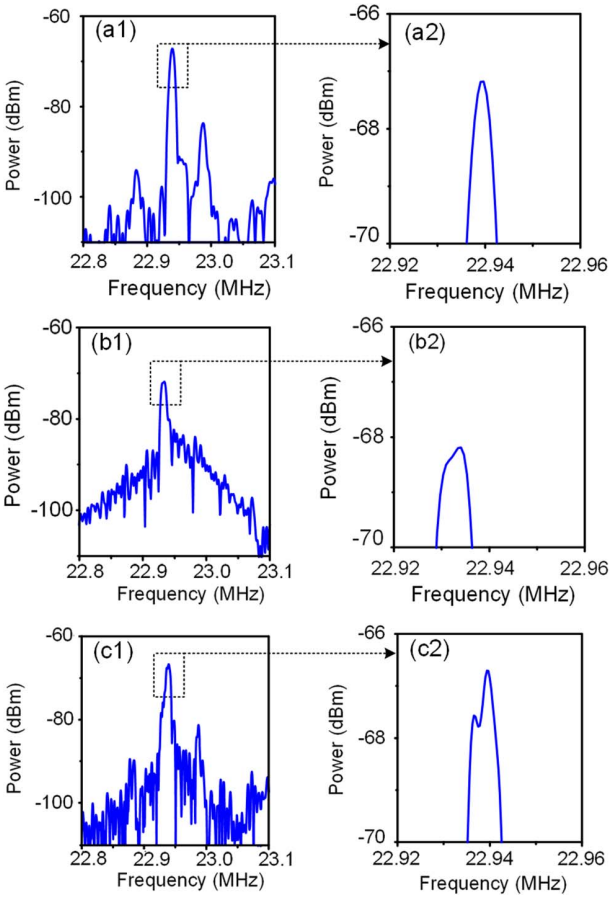

Fig. 8. Spectra of the de-chirped signals generated at (a) channel X and (b) channel Y when two LFM signals with bandwidths of 8.4 GHz are transmitted. (c) The spectrum of the synthetic de-chirped signal. (a2), (b2), (c2) The zoom-in views of (a1), (b1), and (c1).

combined. Figure 8 shows the spectra of the de-chirped signals before and after synthesis. In Fig. 8(c), two peaks located at 22.9366 MHz and 22.9395 MHz can be observed, while only one peak can be seen in Figs. 8(a) and 8(b). The frequency difference between the two peaks is 2.9 kHz, and the calculated distance between the two targets is 1.09 cm, which shows that the two targets can be distinguished with an error of 0.09 cm, very close to the real distance.

In the experiments, the target is close to the radar. In practical application, the target is usually far away from the radar, so the phase error at the combination point caused by the different distances between the target and the antennas of the two channels is small. The time delay between the radar echo and the transmitted signal is enlarged, the frequency of the de-chirped signal increases, and the signal duration becomes short. The shortened signal duration results in a reduction of the synthetic bandwidth. Thanks to the low transmission loss of the optical fiber, we can introduce a large delay to the reference optical signal, as demonstrated in Ref. [18], to reduce the frequency of the de-chirped signal and ensure sufficient equivalent synthetic bandwidth.

In conclusion, we have demonstrated a microwave photonic radar with post-bandwidth synthesis, aiming to achieve ultra-high range resolution detection using RF frontends and antennas with relatively small bandwidth. Because only one laser is used and polarization multiplexing is introduced, the proposed system is compact and cost effective. In the proof-of-concept experiment, two signals de-chirped from two LFM signals with a bandwidth of 8.4 GHz were combined into one signal as if de-chirped from an LFM signal with a bandwidth of 16 GHz, and a range resolution of 1 cm was obtained.

This work was supported in part by the National Key R&D Program of China (No. 2018YFB2201803), the National Natural Science Foundation of China (No. 61804159), and the Natural Science Foundation of Jiangsu Province (No. BK20160802).

References

1. M. I. Skolnik, *Radar Handbook* (McGraw-Hill, 2008).
2. F. Gini, A. De Maio, and L. Patton, *Waveform Design and Diversity for Advanced Radar Systems* (Institution of Engineering and Technology, 2012).
3. M. A. Richards, *Fundamentals of Radar Signal Processing* (McGraw-Hill, 2014).
4. J. Capmany and D. Novak, Nat. Photon. **1**, 319 (2007).
5. J. Yao, J. Lightw. Technol. **27**, 314 (2009).
6. P. Ghelfi, F. Laghezza, F. Scotti, G. Serafino, S. Pinna, D. Onori, E. Lazzeri, and A. Bogoni, IEEE Microw. Mag. **16**, 74 (2015).
7. J. Yang, S. Li, X. Xiao, D. Wu, X. Xue, and X. Zheng, Chin. Opt. Lett. **16**, 060605 (2018).
8. T. H. Du, D. Zhu, and S. L. Pan, Chin. Opt. Lett. **16**, 010604 (2018).
9. G. Serafino, F. Scotti, L. Lembo, B. Hussain, C. Porzi, A. Malacarne, S. Maresca, D. Onori, P. Ghelfi, and A. Bogoni, J. Lightwave Technol. **37**, 643 (2019).
10. J. Cao, R. Li, J. Yang, Z. Mo, J. Dong, X. Zhang, W. Jiang, and W. Li, J. Lightwave Technol. **37**, 2403 (2019).
11. X. Ye, F. Zhang, Y. Yang, and S. Pan, Photon. Res. **7**, 265 (2019).
12. X. C. Wang, S. P. Li, X. Jiang, J. T. Hu, S. Z. Xu, M. Xue, and S. L. Pan, Chin. Opt. Lett. **17**, 060601 (2019).
13. N. Shi, W. Li, N. Zhu, and M. Li, Chin. Opt. Lett. **17**, 052301 (2019).
14. Y. Li, A. Rashidinejad, J. M. Wun, D. E. Leaird, J. W. Shi, and A. M. Weiner, Optica **1**, 446 (2014).
15. S. Zhang, W. Zou, N. Qian, and J. Chen, IEEE Photon. Technol. Lett. **30**, 1028 (2018).
16. S. Wang, H. Zhang, S. Jia, M. Saqlain, S. Zheng, H. Chi, X. Jin, X. Zhang, and X. Yu, IEEE Photon. Technol. Lett. **30**, 1760 (2018).
17. S. Peng, S. Li, X. Xue, X. Xiao, D. Wu, X. Zheng, and B. Zhou, Opt. Express **26**, 1978 (2018).
18. A. Wang, J. Wo, X. Luo, Y. Wang, W. Cong, P. Du, J. Zhang, B. Zhao, J. Zhang, Y. Zhu, J. Lan, and L. Yu, Opt. Express **26**, 20708 (2018).
19. R. Li, W. Li, M. Ding, Z. Wen, Y. Li, L. Zhou, S. Yu, T. Xing, B. Gao, Y. Luan, Y. Zhu, P. Guo, Y. Tian, and X. Liang, Opt. Express **25**, 14334 (2017).
20. F. Zhang, Q. Guo, Z. Wang, P. Zhou, G. Zhang, J. Sun, and S. Pan, Opt. Express **25**, 16274 (2017).
21. F. Z. Zhang, Q. S. Guo, Y. Zhang, Y. Yao, P. Zhou, D. Y. Zhu, and S. L. Pan, Chin. Opt. Lett. **15**, 112801 (2017).
22. P. Ghelfi, F. Laghezza, F. Scotti, D. Onori, and A. Bogoni, J. Light. Technol. **34**, 500 (2016).
23. S. Peng, S. Li, X. Xue, X. Xiao, D. Wu, and X. Zheng, IEEE Photon. J. **11**, 5502408 (2019).
24. J. Tsao and B. D. Steinberg, IEEE Trans. Antennas Propag. **36**, 543 (1988).
25. J. Salzman, D. Akamine, R. Lefevre, and J. C. Kirk, IEEE Aerosp. Electron. Syst. Mag. **17**, 33 (2002).
26. H. Schimpf, A. Wahlen, and H. Essen, Electron. Lett. **39**, 1346 (2003).
27. X. Nie, D. Zhu, X. Mao, L. Wang, and Z. Zhu, in *IEEE Radar Conference* (2009).
28. X. Zhang, W. Zhai, and Y. Zhang, in *2009 Asia Pacific Microwave Conference* (2009), p. 1208.
29. P. Hu, J. Zou, B. Tian, S. Xu, and Z. Chen, in *Progress in Electromagnetic Research Symposium* (2016), p. 3524.
30. G. B. Jing, G. C. Sun, X. G. Xia, M. D. Xing, and Z. Bao, IEEE Geosci. Remote Sens. Lett. **14**, 2290 (2017).